arXiv:1402.2554v2 [hep-ex] 19 Mar 2014

EUROPEAN ORGANIZATION FOR NUCLEAR RESEARCH (CERN)

CERN-PH-EP-2014-018
LHCb-PAPER-2013-065
March 19, 2014

Measurements of the B^+, B^0, B_s^0 meson and Λ_b^0 baryon lifetimes

The LHCb collaboration[†]

Abstract

Measurements of b-hadron lifetimes are reported using pp collision data, corresponding to an integrated luminosity of $1.0\,\text{fb}^{-1}$, collected by the LHCb detector at a centre-of-mass energy of 7 TeV. Using the exclusive decays $B^+ \to J/\psi K^+$, $B^0 \to J/\psi K^*(892)^0$, $B^0 \to J/\psi K^0_S$, $\Lambda_b^0 \to J/\psi \Lambda$ and $B_s^0 \to J/\psi \phi$ the average decay times in these modes are measured to be

$$\begin{aligned}
\tau_{B^+\to J/\psi K^+} &= 1.637 \pm 0.004 \pm 0.003 \text{ ps},\\
\tau_{B^0\to J/\psi K^{*0}} &= 1.524 \pm 0.006 \pm 0.004 \text{ ps},\\
\tau_{B^0\to J/\psi K^0_S} &= 1.499 \pm 0.013 \pm 0.005 \text{ ps},\\
\tau_{\Lambda_b^0\to J/\psi \Lambda} &= 1.415 \pm 0.027 \pm 0.006 \text{ ps},\\
\tau_{B_s^0\to J/\psi \phi} &= 1.480 \pm 0.011 \pm 0.005 \text{ ps},
\end{aligned}$$

where the first uncertainty is statistical and the second is systematic. These represent the most precise lifetime measurements in these decay modes. In addition, ratios of these lifetimes, and the ratio of the decay-width difference, $\Delta\Gamma_d$, to the average width, Γ_d, in the B^0 system, $\Delta\Gamma_d/\Gamma_d = -0.044 \pm 0.025 \pm 0.011$, are reported. All quantities are found to be consistent with Standard Model expectations.

Submitted to JHEP

© CERN on behalf of the LHCb collaboration, license CC-BY-3.0.

[†]Authors are listed on the following pages.

LHCb collaboration

R. Aaij[40], B. Adeva[36], M. Adinolfi[45], A. Affolder[51], Z. Ajaltouni[5], J. Albrecht[9], F. Alessio[37], M. Alexander[50], S. Ali[40], G. Alkhazov[29], P. Alvarez Cartelle[36], A.A. Alves Jr[24], S. Amato[2], S. Amerio[21], Y. Amhis[7], L. Anderlini[17,g], J. Anderson[39], R. Andreassen[56], M. Andreotti[16,f], J.E. Andrews[57], R.B. Appleby[53], O. Aquines Gutierrez[10], F. Archilli[37], A. Artamonov[34], M. Artuso[58], E. Aslanides[6], G. Auriemma[24,n], M. Baalouch[5], S. Bachmann[11], J.J. Back[47], A. Badalov[35], V. Balagura[30], W. Baldini[16], R.J. Barlow[53], C. Barschel[38], S. Barsuk[7], W. Barter[46], V. Batozskaya[27], Th. Bauer[40], A. Bay[38], J. Beddow[50], F. Bedeschi[22], I. Bediaga[1], S. Belogurov[30], K. Belous[34], I. Belyaev[30], E. Ben-Haim[8], G. Bencivenni[18], S. Benson[49], J. Benton[45], A. Berezhnoy[31], R. Bernet[39], M.-O. Bettler[46], M. van Beuzekom[40], A. Bien[11], S. Bifani[44], T. Bird[53], A. Bizzeti[17,i], P.M. Bjørnstad[53], T. Blake[47], F. Blanc[38], J. Blouw[10], S. Blusk[58], V. Bocci[24], A. Bondar[33], N. Bondar[29], W. Bonivento[15,37], S. Borghi[53], A. Borgia[58], M. Borsato[7], T.J.V. Bowcock[51], E. Bowen[39], C. Bozzi[16], T. Brambach[9], J. van den Brand[41], J. Bressieux[38], D. Brett[53], M. Britsch[10], T. Britton[58], N.H. Brook[45], H. Brown[51], A. Bursche[39], G. Busetto[21,r], J. Buytaert[37], S. Cadeddu[15], R. Calabrese[16,f], O. Callot[7], M. Calvi[20,k], M. Calvo Gomez[35,p], A. Camboni[35], P. Campana[18,37], D. Campora Perez[37], A. Carbone[14,d], G. Carboni[23,l], R. Cardinale[19,j], A. Cardini[15], H. Carranza-Mejia[49], L. Carson[49], K. Carvalho Akiba[2], G. Casse[51], L. Castillo Garcia[37], M. Cattaneo[37], Ch. Cauet[9], R. Cenci[57], M. Charles[8], Ph. Charpentier[37], S.-F. Cheung[54], N. Chiapolini[39], M. Chrzaszcz[39,25], K. Ciba[37], X. Cid Vidal[37], G. Ciezarek[52], P.E.L. Clarke[49], M. Clemencic[37], H.V. Cliff[46], J. Closier[37], C. Coca[28], V. Coco[37], J. Cogan[6], E. Cogneras[5], P. Collins[37], A. Comerma-Montells[35], A. Contu[15,37], A. Cook[45], M. Coombes[45], S. Coquereau[8], G. Corti[37], I. Counts[55], B. Couturier[37], G.A. Cowan[49], D.C. Craik[47], M. Cruz Torres[59], S. Cunliffe[52], R. Currie[49], C. D'Ambrosio[37], J. Dalseno[45], P. David[8], P.N.Y. David[40], A. Davis[56], I. De Bonis[4], K. De Bruyn[40], S. De Capua[53], M. De Cian[11], J.M. De Miranda[1], L. De Paula[2], W. De Silva[56], P. De Simone[18], D. Decamp[4], M. Deckenhoff[9], L. Del Buono[8], N. Déléage[4], D. Derkach[54], O. Deschamps[5], F. Dettori[41], A. Di Canto[11], H. Dijkstra[37], S. Donleavy[51], F. Dordei[11], M. Dorigo[38], P. Dorosz[25,o], A. Dosil Suárez[36], D. Dossett[47], A. Dovbnya[42], F. Dupertuis[38], P. Durante[37], R. Dzhelyadin[34], A. Dziurda[25], A. Dzyuba[29], S. Easo[48], U. Egede[52], V. Egorychev[30], S. Eidelman[33], S. Eisenhardt[49], U. Eitschberger[9], R. Ekelhof[9], L. Eklund[50,37], I. El Rifai[5], Ch. Elsasser[39], S. Esen[11], A. Falabella[16,f], C. Färber[11], C. Farinelli[40], S. Farry[51], D. Ferguson[49], V. Fernandez Albor[36], F. Ferreira Rodrigues[1], M. Ferro-Luzzi[37], S. Filippov[32], M. Fiore[16,f], M. Fiorini[16,f], C. Fitzpatrick[37], M. Fontana[10], F. Fontanelli[19,j], R. Forty[37], O. Francisco[2], M. Frank[37], C. Frei[37], M. Frosini[17,37,g], E. Furfaro[23,l], A. Gallas Torreira[36], D. Galli[14,d], M. Gandelman[2], P. Gandini[58], Y. Gao[3], J. Garofoli[58], J. Garra Tico[46], L. Garrido[35], C. Gaspar[37], R. Gauld[54], E. Gersabeck[11], M. Gersabeck[53], T. Gershon[47], Ph. Ghez[4], A. Gianelle[21], S. Giani'[38], V. Gibson[46], L. Giubega[28], V.V. Gligorov[37], C. Göbel[59], D. Golubkov[30], A. Golutvin[52,30,37], A. Gomes[1,a], H. Gordon[37], M. Grabalosa Gándara[5], R. Graciani Diaz[35], L.A. Granado Cardoso[37], E. Graugés[35], G. Graziani[17], A. Grecu[28], E. Greening[54], S. Gregson[46], P. Griffith[44], L. Grillo[11], O. Grünberg[60], B. Gui[58], E. Gushchin[32], Yu. Guz[34,37], T. Gys[37], C. Hadjivasiliou[58], G. Haefeli[38], C. Haen[37], T.W. Hafkenscheid[62], S.C. Haines[46], S. Hall[52], B. Hamilton[57], T. Hampson[45], S. Hansmann-Menzemer[11], N. Harnew[54], S.T. Harnew[45], J. Harrison[53], T. Hartmann[60], J. He[37], T. Head[37], V. Heijne[40], K. Hennessy[51], P. Henrard[5], J.A. Hernando Morata[36], E. van Herwijnen[37], M. Heß[60], A. Hicheur[1], D. Hill[54], M. Hoballah[5], C. Hombach[53], W. Hulsbergen[40], P. Hunt[54], N. Hussain[54], D. Hutchcroft[51],

D. Hynds[50], V. Iakovenko[43], M. Idzik[26], P. Ilten[55], R. Jacobsson[37], A. Jaeger[11], E. Jans[40], P. Jaton[38], A. Jawahery[57], F. Jing[3], M. John[54], D. Johnson[54], C.R. Jones[46], C. Joram[37], B. Jost[37], N. Jurik[58], M. Kaballo[9], S. Kandybei[42], W. Kanso[6], M. Karacson[37], T.M. Karbach[37], I.R. Kenyon[44], T. Ketel[41], B. Khanji[20], C. Khurewathanakul[38], S. Klaver[53], O. Kochebina[7], I. Komarov[38], R.F. Koopman[41], P. Koppenburg[40], M. Korolev[31], A. Kozlinskiy[40], L. Kravchuk[32], K. Kreplin[11], M. Kreps[47], G. Krocker[11], P. Krokovny[33], F. Kruse[9], M. Kucharczyk[20,25,37,k], V. Kudryavtsev[33], K. Kurek[27], T. Kvaratskheliya[30,37], V.N. La Thi[38], D. Lacarrere[37], G. Lafferty[53], A. Lai[15], D. Lambert[49], R.W. Lambert[41], E. Lanciotti[37], G. Lanfranchi[18], C. Langenbruch[37], T. Latham[47], C. Lazzeroni[44], R. Le Gac[6], J. van Leerdam[40], J.-P. Lees[4], R. Lefèvre[5], A. Leflat[31], J. Lefrançois[7], S. Leo[22], O. Leroy[6], T. Lesiak[25], B. Leverington[11], Y. Li[3], M. Liles[51], R. Lindner[37], C. Linn[11], F. Lionetto[39], B. Liu[15], G. Liu[37], S. Lohn[37], I. Longstaff[50], J.H. Lopes[2], N. Lopez-March[38], P. Lowdon[39], H. Lu[3], D. Lucchesi[21,r], J. Luisier[38], H. Luo[49], E. Luppi[16,f], O. Lupton[54], F. Machefert[7], I.V. Machikhiliyan[30], F. Maciuc[28], O. Maev[29,37], S. Malde[54], G. Manca[15,e], G. Mancinelli[6], M. Manzali[16,f], J. Maratas[5], U. Marconi[14], P. Marino[22,t], R. Märki[38], J. Marks[11], G. Martellotti[24], A. Martens[8], A. Martín Sánchez[7], M. Martinelli[40], D. Martinez Santos[41], D. Martins Tostes[2], A. Massafferri[1], R. Matev[37], Z. Mathe[37], C. Matteuzzi[20], A. Mazurov[16,37,f], M. McCann[52], J. McCarthy[44], A. McNab[53], R. McNulty[12], B. McSkelly[51], B. Meadows[56,54], F. Meier[9], M. Meissner[11], M. Merk[40], D.A. Milanes[8], M.-N. Minard[4], J. Molina Rodriguez[59], S. Monteil[5], D. Moran[53], M. Morandin[21], P. Morawski[25], A. Mordà[6], M.J. Morello[22,t], R. Mountain[58], F. Muheim[49], K. Müller[39], R. Muresan[28], B. Muryn[26], B. Muster[38], P. Naik[45], T. Nakada[38], R. Nandakumar[48], I. Nasteva[1], M. Needham[49], S. Neubert[37], N. Neufeld[37], A.D. Nguyen[38], T.D. Nguyen[38], C. Nguyen-Mau[38,q], M. Nicol[7], V. Niess[5], R. Niet[9], N. Nikitin[31], T. Nikodem[11], A. Novoselov[34], A. Oblakowska-Mucha[26], V. Obraztsov[34], S. Oggero[40], S. Ogilvy[50], O. Okhrimenko[43], R. Oldeman[15,e], G. Onderwater[62], M. Orlandea[28], J.M. Otalora Goicochea[2], P. Owen[52], A. Oyanguren[35], B.K. Pal[58], A. Palano[13,c], M. Palutan[18], J. Panman[37], A. Papanestis[48,37], M. Pappagallo[50], L. Pappalardo[16], C. Parkes[53], C.J. Parkinson[9], G. Passaleva[17], G.D. Patel[51], M. Patel[52], C. Patrignani[19,j], C. Pavel-Nicorescu[28], A. Pazos Alvarez[36], A. Pearce[53], A. Pellegrino[40], G. Penso[24,m], M. Pepe Altarelli[37], S. Perazzini[14,d], E. Perez Trigo[36], P. Perret[5], M. Perrin-Terrin[6], L. Pescatore[44], E. Pesen[63], G. Pessina[20], K. Petridis[52], A. Petrolini[19,j], E. Picatoste Olloqui[35], B. Pietrzyk[4], T. Pilař[47], D. Pinci[24], A. Pistone[19], S. Playfer[49], M. Plo Casasus[36], F. Polci[8], G. Polok[25], A. Poluektov[47,33], E. Polycarpo[2], A. Popov[34], D. Popov[10], B. Popovici[28], C. Potterat[35], A. Powell[54], J. Prisciandaro[38], A. Pritchard[51], C. Prouve[45], V. Pugatch[43], A. Puig Navarro[38], G. Punzi[22,s], W. Qian[4], B. Rachwal[25], J.H. Rademacker[45], B. Rakotomiaramanana[38], M. Rama[18], M.S. Rangel[2], I. Raniuk[42], N. Rauschmayr[37], G. Raven[41], S. Redford[54], S. Reichert[53], M.M. Reid[47], A.C. dos Reis[1], S. Ricciardi[48], A. Richards[52], K. Rinnert[51], V. Rives Molina[35], D.A. Roa Romero[5], P. Robbe[7], D.A. Roberts[57], A.B. Rodrigues[1], E. Rodrigues[53], P. Rodriguez Perez[36], S. Roiser[37], V. Romanovsky[34], A. Romero Vidal[36], M. Rotondo[21], J. Rouvinet[38], T. Ruf[37], F. Ruffini[22], H. Ruiz[35], P. Ruiz Valls[35], G. Sabatino[24,l], J.J. Saborido Silva[36], N. Sagidova[29], P. Sail[50], B. Saitta[15,e], V. Salustino Guimaraes[2], B. Sanmartin Sedes[36], R. Santacesaria[24], C. Santamarina Rios[36], E. Santovetti[23,l], M. Sapunov[6], A. Sarti[18], C. Satriano[24,n], A. Satta[23], M. Savrie[16,f], D. Savrina[30,31], M. Schiller[41], H. Schindler[37], M. Schlupp[9], M. Schmelling[10], B. Schmidt[37], O. Schneider[38], A. Schopper[37], M.-H. Schune[7], R. Schwemmer[37], B. Sciascia[18], A. Sciubba[24], M. Seco[36], A. Semennikov[30], K. Senderowska[26], I. Sepp[52], N. Serra[39], J. Serrano[6], P. Seyfert[11], M. Shapkin[34], I. Shapoval[16,42,f], Y. Shcheglov[29], T. Shears[51], L. Shekhtman[33],

O. Shevchenko[42], V. Shevchenko[61], A. Shires[9], R. Silva Coutinho[47], G. Simi[21], M. Sirendi[46], N. Skidmore[45], T. Skwarnicki[58], N.A. Smith[51], E. Smith[54,48], E. Smith[52], J. Smith[46], M. Smith[53], H. Snoek[40], M.D. Sokoloff[56], F.J.P. Soler[50], F. Soomro[38], D. Souza[45], B. Souza De Paula[2], B. Spaan[9], A. Sparkes[49], F. Spinella[22], P. Spradlin[50], F. Stagni[37], S. Stahl[11], O. Steinkamp[39], S. Stevenson[54], S. Stoica[28], S. Stone[58], B. Storaci[39], S. Stracka[22,37], M. Straticiuc[28], U. Straumann[39], R. Stroili[21], V.K. Subbiah[37], L. Sun[56], W. Sutcliffe[52], S. Swientek[9], V. Syropoulos[41], M. Szczekowski[27], P. Szczypka[38,37], D. Szilard[2], T. Szumlak[26], S. T'Jampens[4], M. Teklishyn[7], G. Tellarini[16,f], E. Teodorescu[28], F. Teubert[37], C. Thomas[54], E. Thomas[37], J. van Tilburg[11], V. Tisserand[4], M. Tobin[38], S. Tolk[41], L. Tomassetti[16,f], D. Tonelli[37], S. Topp-Joergensen[54], N. Torr[54], E. Tournefier[4,52], S. Tourneur[38], M.T. Tran[38], M. Tresch[39], A. Tsaregorodtsev[6], P. Tsopelas[40], N. Tuning[40], M. Ubeda Garcia[37], A. Ukleja[27], A. Ustyuzhanin[61], U. Uwer[11], V. Vagnoni[14], G. Valenti[14], A. Vallier[7], R. Vazquez Gomez[18], P. Vazquez Regueiro[36], C. Vázquez Sierra[36], S. Vecchi[16], J.J. Velthuis[45], M. Veltri[17,h], G. Veneziano[38], M. Vesterinen[11], B. Viaud[7], D. Vieira[2], X. Vilasis-Cardona[35,p], A. Vollhardt[39], D. Volyanskyy[10], D. Voong[45], A. Vorobyev[29], V. Vorobyev[33], C. Voß[60], H. Voss[10], J.A. de Vries[40], R. Waldi[60], C. Wallace[47], R. Wallace[12], S. Wandernoth[11], J. Wang[58], D.R. Ward[46], N.K. Watson[44], A.D. Webber[53], D. Websdale[52], M. Whitehead[47], J. Wicht[37], J. Wiechczynski[25], D. Wiedner[11], L. Wiggers[40], G. Wilkinson[54], M.P. Williams[47,48], M. Williams[55], F.F. Wilson[48], J. Wimberley[57], J. Wishahi[9], W. Wislicki[27], M. Witek[25], G. Wormser[7], S.A. Wotton[46], S. Wright[46], S. Wu[3], K. Wyllie[37], Y. Xie[49,37], Z. Xing[58], Z. Yang[3], X. Yuan[3], O. Yushchenko[34], M. Zangoli[14], M. Zavertyaev[10,b], F. Zhang[3], L. Zhang[58], W.C. Zhang[12], Y. Zhang[3], A. Zhelezov[11], A. Zhokhov[30], L. Zhong[3], A. Zvyagin[37].

[1] *Centro Brasileiro de Pesquisas Físicas (CBPF), Rio de Janeiro, Brazil*
[2] *Universidade Federal do Rio de Janeiro (UFRJ), Rio de Janeiro, Brazil*
[3] *Center for High Energy Physics, Tsinghua University, Beijing, China*
[4] *LAPP, Université de Savoie, CNRS/IN2P3, Annecy-Le-Vieux, France*
[5] *Clermont Université, Université Blaise Pascal, CNRS/IN2P3, LPC, Clermont-Ferrand, France*
[6] *CPPM, Aix-Marseille Université, CNRS/IN2P3, Marseille, France*
[7] *LAL, Université Paris-Sud, CNRS/IN2P3, Orsay, France*
[8] *LPNHE, Université Pierre et Marie Curie, Université Paris Diderot, CNRS/IN2P3, Paris, France*
[9] *Fakultät Physik, Technische Universität Dortmund, Dortmund, Germany*
[10] *Max-Planck-Institut für Kernphysik (MPIK), Heidelberg, Germany*
[11] *Physikalisches Institut, Ruprecht-Karls-Universität Heidelberg, Heidelberg, Germany*
[12] *School of Physics, University College Dublin, Dublin, Ireland*
[13] *Sezione INFN di Bari, Bari, Italy*
[14] *Sezione INFN di Bologna, Bologna, Italy*
[15] *Sezione INFN di Cagliari, Cagliari, Italy*
[16] *Sezione INFN di Ferrara, Ferrara, Italy*
[17] *Sezione INFN di Firenze, Firenze, Italy*
[18] *Laboratori Nazionali dell'INFN di Frascati, Frascati, Italy*
[19] *Sezione INFN di Genova, Genova, Italy*
[20] *Sezione INFN di Milano Bicocca, Milano, Italy*
[21] *Sezione INFN di Padova, Padova, Italy*
[22] *Sezione INFN di Pisa, Pisa, Italy*
[23] *Sezione INFN di Roma Tor Vergata, Roma, Italy*
[24] *Sezione INFN di Roma La Sapienza, Roma, Italy*
[25] *Henryk Niewodniczanski Institute of Nuclear Physics Polish Academy of Sciences, Kraków, Poland*
[26] *AGH - University of Science and Technology, Faculty of Physics and Applied Computer Science,*

Kraków, Poland
[27] *National Center for Nuclear Research (NCBJ), Warsaw, Poland*
[28] *Horia Hulubei National Institute of Physics and Nuclear Engineering, Bucharest-Magurele, Romania*
[29] *Petersburg Nuclear Physics Institute (PNPI), Gatchina, Russia*
[30] *Institute of Theoretical and Experimental Physics (ITEP), Moscow, Russia*
[31] *Institute of Nuclear Physics, Moscow State University (SINP MSU), Moscow, Russia*
[32] *Institute for Nuclear Research of the Russian Academy of Sciences (INR RAN), Moscow, Russia*
[33] *Budker Institute of Nuclear Physics (SB RAS) and Novosibirsk State University, Novosibirsk, Russia*
[34] *Institute for High Energy Physics (IHEP), Protvino, Russia*
[35] *Universitat de Barcelona, Barcelona, Spain*
[36] *Universidad de Santiago de Compostela, Santiago de Compostela, Spain*
[37] *European Organization for Nuclear Research (CERN), Geneva, Switzerland*
[38] *Ecole Polytechnique Fédérale de Lausanne (EPFL), Lausanne, Switzerland*
[39] *Physik-Institut, Universität Zürich, Zürich, Switzerland*
[40] *Nikhef National Institute for Subatomic Physics, Amsterdam, The Netherlands*
[41] *Nikhef National Institute for Subatomic Physics and VU University Amsterdam, Amsterdam, The Netherlands*
[42] *NSC Kharkiv Institute of Physics and Technology (NSC KIPT), Kharkiv, Ukraine*
[43] *Institute for Nuclear Research of the National Academy of Sciences (KINR), Kyiv, Ukraine*
[44] *University of Birmingham, Birmingham, United Kingdom*
[45] *H.H. Wills Physics Laboratory, University of Bristol, Bristol, United Kingdom*
[46] *Cavendish Laboratory, University of Cambridge, Cambridge, United Kingdom*
[47] *Department of Physics, University of Warwick, Coventry, United Kingdom*
[48] *STFC Rutherford Appleton Laboratory, Didcot, United Kingdom*
[49] *School of Physics and Astronomy, University of Edinburgh, Edinburgh, United Kingdom*
[50] *School of Physics and Astronomy, University of Glasgow, Glasgow, United Kingdom*
[51] *Oliver Lodge Laboratory, University of Liverpool, Liverpool, United Kingdom*
[52] *Imperial College London, London, United Kingdom*
[53] *School of Physics and Astronomy, University of Manchester, Manchester, United Kingdom*
[54] *Department of Physics, University of Oxford, Oxford, United Kingdom*
[55] *Massachusetts Institute of Technology, Cambridge, MA, United States*
[56] *University of Cincinnati, Cincinnati, OH, United States*
[57] *University of Maryland, College Park, MD, United States*
[58] *Syracuse University, Syracuse, NY, United States*
[59] *Pontifícia Universidade Católica do Rio de Janeiro (PUC-Rio), Rio de Janeiro, Brazil, associated to* [2]
[60] *Institut für Physik, Universität Rostock, Rostock, Germany, associated to* [11]
[61] *National Research Centre Kurchatov Institute, Moscow, Russia, associated to* [30]
[62] *KVI - University of Groningen, Groningen, The Netherlands, associated to* [40]
[63] *Celal Bayar University, Manisa, Turkey, associated to* [37]

[a] *Universidade Federal do Triângulo Mineiro (UFTM), Uberaba-MG, Brazil*
[b] *P.N. Lebedev Physical Institute, Russian Academy of Science (LPI RAS), Moscow, Russia*
[c] *Università di Bari, Bari, Italy*
[d] *Università di Bologna, Bologna, Italy*
[e] *Università di Cagliari, Cagliari, Italy*
[f] *Università di Ferrara, Ferrara, Italy*
[g] *Università di Firenze, Firenze, Italy*
[h] *Università di Urbino, Urbino, Italy*
[i] *Università di Modena e Reggio Emilia, Modena, Italy*
[j] *Università di Genova, Genova, Italy*
[k] *Università di Milano Bicocca, Milano, Italy*
[l] *Università di Roma Tor Vergata, Roma, Italy*

[m] *Università di Roma La Sapienza, Roma, Italy*
[n] *Università della Basilicata, Potenza, Italy*
[o] *AGH - University of Science and Technology, Faculty of Computer Science, Electronics and Telecommunications, Kraków, Poland*
[p] *LIFAELS, La Salle, Universitat Ramon Llull, Barcelona, Spain*
[q] *Hanoi University of Science, Hanoi, Viet Nam*
[r] *Università di Padova, Padova, Italy*
[s] *Università di Pisa, Pisa, Italy*
[t] *Scuola Normale Superiore, Pisa, Italy*

1 Introduction

Within the framework of heavy quark expansion (HQE) theory [1–7], b-hadron observables are calculated as a perturbative expansion in inverse powers of the b-quark mass, m_b. At zeroth order the lifetimes of all weakly decaying b hadrons are equal, with corrections appearing at order $1/m_b^2$. Ratios of b-hadron lifetimes can be theoretically predicted with higher accuracy than absolute lifetimes since many terms in the HQE cancel. The latest theoretical predictions and world-average values for the b-hadron lifetimes and lifetime ratios are reported in Table 1. A measurement of the ratio of the Λ_b^0 baryon lifetime, using the $\Lambda_b^0 \to J/\psi p K^-$ decay mode[1], to that of the B^0 meson lifetime has recently been made by the LHCb collaboration [8] and is not yet included in the world average.

In this paper, a measurement of the lifetimes of the B^+, B^0 and B_s^0 mesons and Λ_b^0 baryon is reported using pp collision data, corresponding to an integrated luminosity of $1.0\,\text{fb}^{-1}$, collected in 2011 with the LHCb detector at a centre-of-mass energy of 7 TeV. The lifetimes are measured from the reconstructed b-hadron decay time distributions of the exclusive decay modes $B^+ \to J/\psi K^+$, $B^0 \to J/\psi K^*(892)^0$, $B^0 \to J/\psi K_S^0$, $B_s^0 \to J/\psi \phi$ and $\Lambda_b^0 \to J/\psi \Lambda$. Collectively, these are referred to as $H_b \to J/\psi X$ decays. In addition, measurements of lifetime ratios are reported.

As a result of neutral meson mixing the decay time distribution of neutral B_q^0 mesons ($q \in \{s, d\}$) is characterised by two parameters, namely the average decay width Γ_q and the decay width difference $\Delta\Gamma_q$ between the light (L) and heavy (H) B_q^0 mass eigenstates. The summed decay rate of B_q^0 and $\overline{B}{}_q^0$ mesons to a final state f is given by [9–11]

$$\langle \Gamma(B_q^0(t) \to f) \rangle \equiv \Gamma(B_q^0(t) \to f) + \Gamma(\overline{B}{}_q^0(t) \to f) = R_{q,\text{L}}^f e^{-\Gamma_{q,\text{L}} t} + R_{q,\text{H}}^f e^{-\Gamma_{q,\text{H}} t}, \quad (1)$$

where terms proportional to the small flavour specific asymmetry, a_{fs}^q, are ignored [12]. Therefore, for non-zero $\Delta\Gamma_q$ the decay time distribution of neutral B_q^0 decays is not purely exponential. In the case of an equal admixture of B_q^0 and $\overline{B}{}_q^0$ at $t = 0$, the observed average decay time is given by [11]

$$\tau_{B_q^0 \to f} = \frac{1}{\Gamma_q} \frac{1}{1 - y_q^2} \left(\frac{1 + 2\mathcal{A}_{\Delta\Gamma_q}^f y_q + y_q^2}{1 + \mathcal{A}_{\Delta\Gamma_q}^f y_q} \right), \quad (2)$$

where $y_q \equiv \Delta\Gamma_q/(2\Gamma_q)$ and $\mathcal{A}_{\Delta\Gamma_q}^f \equiv (R_{q,\text{H}}^f - R_{q,\text{L}}^f)/(R_{q,\text{H}}^f + R_{q,\text{L}}^f)$ is an observable that depends on the final state, f. As such, the lifetimes measured are usually referred to as *effective* lifetimes. In the B_s^0 system, where $\Delta\Gamma_s/\Gamma_s = 0.159 \pm 0.023$ [13], the deviation from an exponential decay time distribution is non-negligible. In contrast, in the B^0 system this effect is expected to be small as $\Delta\Gamma_d/\Gamma_d$ is predicted to be $(42 \pm 8) \times 10^{-4}$ in the Standard Model (SM) [14, 15]. Both the BaBar [16, 17] and Belle [18] collaborations have measured $|\Delta\Gamma_d/\Gamma_d|$ and the current world average is $|\Delta\Gamma_d/\Gamma_d| = 0.015 \pm 0.018$ [13]. A deviation in the value of $\Delta\Gamma_d$ from the SM prediction has recently been proposed [19] as

[1] Charge conjugation is implied throughout this paper, unless otherwise stated.

Table 1: Theoretical predictions and current world-average values [13] for b-hadron lifetimes and lifetime ratios.

Observable	Prediction	World average
τ_{B^+}[ps]	–	1.641 ± 0.008
τ_{B^0}[ps]	–	1.519 ± 0.007
$\tau_{B_s^0}$[ps]	–	1.516 ± 0.011
$\tau_{\Lambda_b^0}$[ps]	–	1.429 ± 0.024
τ_{B^+}/τ_{B^0}	1.063 ± 0.027 [15, 22, 23]	1.079 ± 0.007
$\tau_{B_s^0}/\tau_{B^0}$	1.00 ± 0.01 [15, 23–25]	0.998 ± 0.009
$\tau_{\Lambda_b^0}/\tau_{B^0}$	0.86–0.95 [3, 23, 26–32]	0.941 ± 0.016

a potential explanation for the anomalous like-sign dimuon charge asymmetry measured by the D0 collaboration [20]. In this paper, $\Delta\Gamma_d/\Gamma_d$ is measured from the effective lifetimes of $B^0 \to J/\psi\, K^*(892)^0$ and $B^0 \to J/\psi\, K^0_{\rm S}$ decays, as proposed in Ref. [21].

The main challenge in the measurements reported is understanding and controlling the detector acceptance, reconstruction and selection efficiencies that depend upon the b-hadron decay time. This paper is organised as follows. Section 2 describes the LHCb detector and software. The selection criteria for the b-hadron candidates are described in Sec. 3. Section 4 describes the reconstruction efficiencies and the techniques used to correct the decay time distributions. Section 5 describes how the efficiency corrections are incorporated into the maximum likelihood fit that is used to measure the signal yields and lifetimes. The systematic uncertainties on the measurements are described in Sec. 6. The final results and conclusions are presented in Sec. 7.

2 Detector and software

The LHCb detector [33] is a single-arm forward spectrometer covering the pseudorapidity range $2 < \eta < 5$, designed for the study of particles containing b or c quarks. The detector includes a high-precision tracking system consisting of a silicon-strip vertex detector (VELO) surrounding the pp interaction region, a large-area silicon-strip detector (TT) located upstream of a dipole magnet with a bending power of about 4 Tm, and three stations of silicon-strip detectors and straw drift tubes placed downstream. The combined tracking system provides a momentum, p, measurement with relative uncertainty that varies from 0.4% at 5 GeV/c to 0.6% at 100 GeV/c, and impact parameter resolution of 20 µm for charged particles with high transverse momentum, $p_{\rm T}$. Charged hadrons are identified using two ring-imaging Cherenkov detectors [34]. Photon, electron and hadron candidates are identified by a calorimeter system consisting of scintillating-pad and preshower detectors, an electromagnetic calorimeter and a hadronic calorimeter. Muons are identified by a system composed of alternating layers of iron and multiwire proportional chambers [35]. The right-handed coordinate system adopted has the z-axis along the beam line and the y-axis along the vertical. The trigger [36] consists of a hardware stage,

based on information from the calorimeter and muon systems, followed by a software stage, which applies a full event reconstruction.

Two distinct classes of tracks are reconstructed using hits in the tracking stations on both sides of the magnet, either with hits in the VELO (long track) or without (downstream track). The vertex resolution of b-hadron candidates reconstructed using long tracks is better than that for candidates reconstructed using downstream tracks. However, the use of long tracks introduces a dependence of the reconstruction efficiency on the b-hadron decay time.

In the simulation, pp collisions are generated using PYTHIA 6.4 [37] with a specific LHCb configuration [38]. Decays of hadronic particles are described by EVTGEN [39], in which final state radiation is generated using PHOTOS [40]. The interaction of the generated particles with the detector and its response are implemented using the GEANT4 toolkit [41] as described in Ref. [42].

3 Candidate selection

The reconstruction of each of the $H_b \to J/\psi X$ decays is similar and commences by selecting $J/\psi \to \mu^+\mu^-$ decays. Events passing the hardware trigger contain dimuon candidates with high transverse momentum. The subsequent software trigger is composed of two stages. The first stage performs a partial event reconstruction and requires events to have two well-identified oppositely charged muons with an invariant mass larger than $2.7\,\mathrm{GeV}/c^2$. The selection at this stage has a uniform efficiency as a function of decay time. The second stage performs a full event reconstruction, calculating the position of each pp interaction vertex (PV) using all available charged particles in the event. The average number of PVs in each event is approximately 2.0. Their longitudinal (z) position is known to a precision of approximately 0.05 mm. If multiple PVs are reconstructed in the event, the one with the minimum value of $\chi^2_{\rm IP}$ is associated with the J/ψ candidate, where $\chi^2_{\rm IP}$ is the increase in the χ^2 of the PV fit if the candidate trajectory is included. Events are retained for further processing if they contain a $J/\psi \to \mu^+\mu^-$ pair that forms a vertex that is significantly displaced from the PV. This introduces a non-uniform efficiency as function of decay time.

The offline sample of J/ψ meson candidates is selected by requiring each muon to have $p_{\rm T}$ larger than $500\,\mathrm{MeV}/c$ and the J/ψ candidate to be displaced from the PV by more than three times its decay length uncertainty. The invariant mass of the two muons, $m(\mu^+\mu^-)$, must be in the range $[3030, 3150]\,\mathrm{MeV}/c^2$.

The b-hadron candidate selection is performed by applying kinematic and particle identification criteria to the final-state tracks, the details of which are reported in Sec. 3.1 to 3.5. No requirements are placed on variables that are highly correlated to the b-hadron decay time, thereby avoiding the introduction of additional biases. All final-state particles are required to have a pseudorapidity in the range $2.0 < \eta < 4.5$. In addition, the z-position of the PV ($z_{\rm PV}$) is required to be within 100 mm of the nominal interaction point, where the standard deviation of the $z_{\rm PV}$ distribution is approximately 47 mm. These criteria cause a reduction of approximately 10% in signal yield but define a fiducial region where

the reconstruction efficiency is largely uniform.

The maximum likelihood fit uses the invariant mass, $m(J/\psi X)$, and proper decay time, t, of each b-hadron candidate. The decay time of the b-hadron candidate in its rest frame is derived from the relation $t = m\,l/q$, where m is its invariant mass and the decay length, l, and the momentum, q, are measured in the experimental frame. In this paper, t is computed using a kinematic decay-tree fit (DTF) [43] involving all final-state tracks from the b-hadron candidate with a constraint on the position of the associated PV. Unlike in the trigger, the position of each PV is calculated using all available charged particles in the event after the removal of the b-hadron candidate final-state tracks. This is necessary to prevent the final-state tracks from biasing the PV position towards the b-hadron decay vertex and helps to reduce the tails of the decay-time resolution function. This prescription does not bias the measured lifetime using simulated events. The χ^2 of the fit, $\chi^2_{\rm DTF}$, is useful to discriminate between signal and background. In cases where there are multiple b-hadron candidates per event, the candidate with the smallest $\chi^2_{\rm DTF}$ is chosen. The z-position of the displaced b-hadron vertices are known to a precision of approximately 0.15 mm.

Studies of simulated events show that in the case of $B^0 \to J/\psi\,K^{*0}$ ($B^0_s \to J/\psi\,\phi$) decays, imposing requirements on $\chi^2_{\rm DTF}$ introduces a dependence of the selection efficiency on the decay time if the K^+ and π^- (K^+ and K^-) tracks are included in the DTF. If no correction is applied to the decay time distribution, the measured lifetime would be biased by approximately -2 fs relative to the generated value. Using simulated events it is found that this effect is correlated to the opening angle between the K^+ and π^- (K^+ and K^-) from the K^{*0} (ϕ) decay. No effect is observed for the muons coming from the J/ψ decay due to the larger opening angle in this case. To remove the effect, the calculation of $\chi^2_{\rm DTF}$ for the $B^0 \to J/\psi\,K^{*0}$ and $B^0_s \to J/\psi\,\phi$ channels is performed with an alternative DTF in which the assigned track parameter uncertainties of the kaon and pion are increased in such a way that their contribution to the b-hadron vertex position is negligible.

Candidates are required to have t in the range $[0.3, 14.0]$ ps. The lower bound on the decay time suppresses a large fraction of the prompt combinatorial background that is composed of tracks from the same PV, while the upper bound is introduced to reduce the sensitivity to long-lived background candidates. In the case of the $B^0 \to J/\psi\,K^0_{\rm S}$ and $\Lambda^0_b \to J/\psi\,\Lambda$ decays, the lower bound is increased to 0.45 ps to compensate for the worse decay time resolution in these modes.

In events with multiple PVs, b-hadron candidates are removed if they have a $\chi^2_{\rm IP}$ with respect to the next best PV smaller than 50. This requirement is found to distort the decay time distribution, but reduces a source of background due to the incorrect association of the b hadron to its production PV.

The invariant mass is computed using another kinematic fit without any constraint on the PV position but with the invariant mass of the $\mu^+\mu^-$ pair, $m(\mu^+\mu^-)$, constrained to the known J/ψ mass [44]. Figures 1 and 2 show the $m(J/\psi X)$ distributions for the selected candidates in each final state and Table 2 gives the corresponding signal yields.

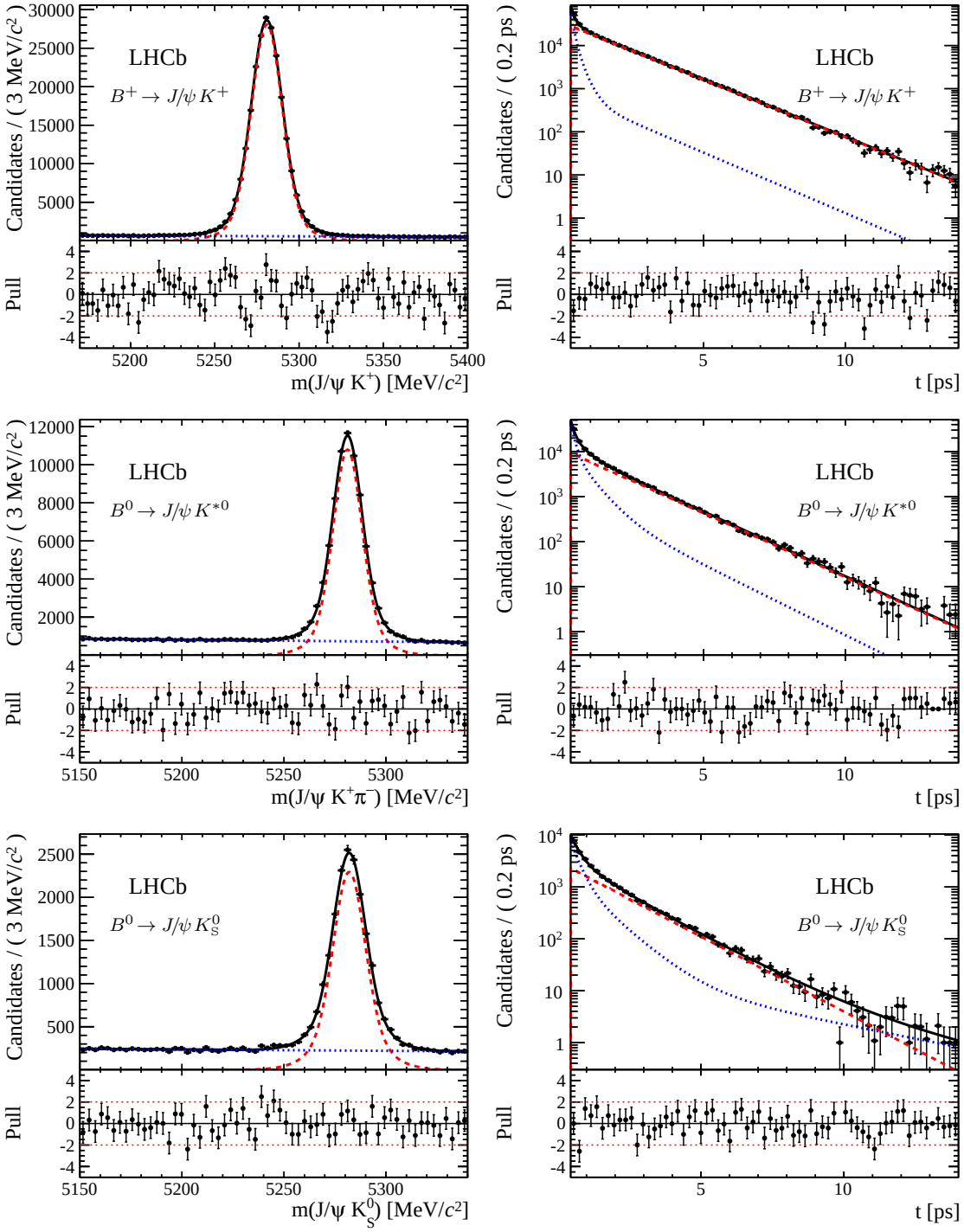

Figure 1: Distributions of the (left) mass and (right) decay time of $B^+ \to J/\psi K^+$, $B^0 \to J/\psi K^{*0}$ and $B^0 \to J/\psi K^0_S$ candidates and their associated residual uncertainties (pulls). The data are shown by the black points; the total fit function by the black solid line; the signal contribution by the red dashed line and the background contribution by the blue dotted line.

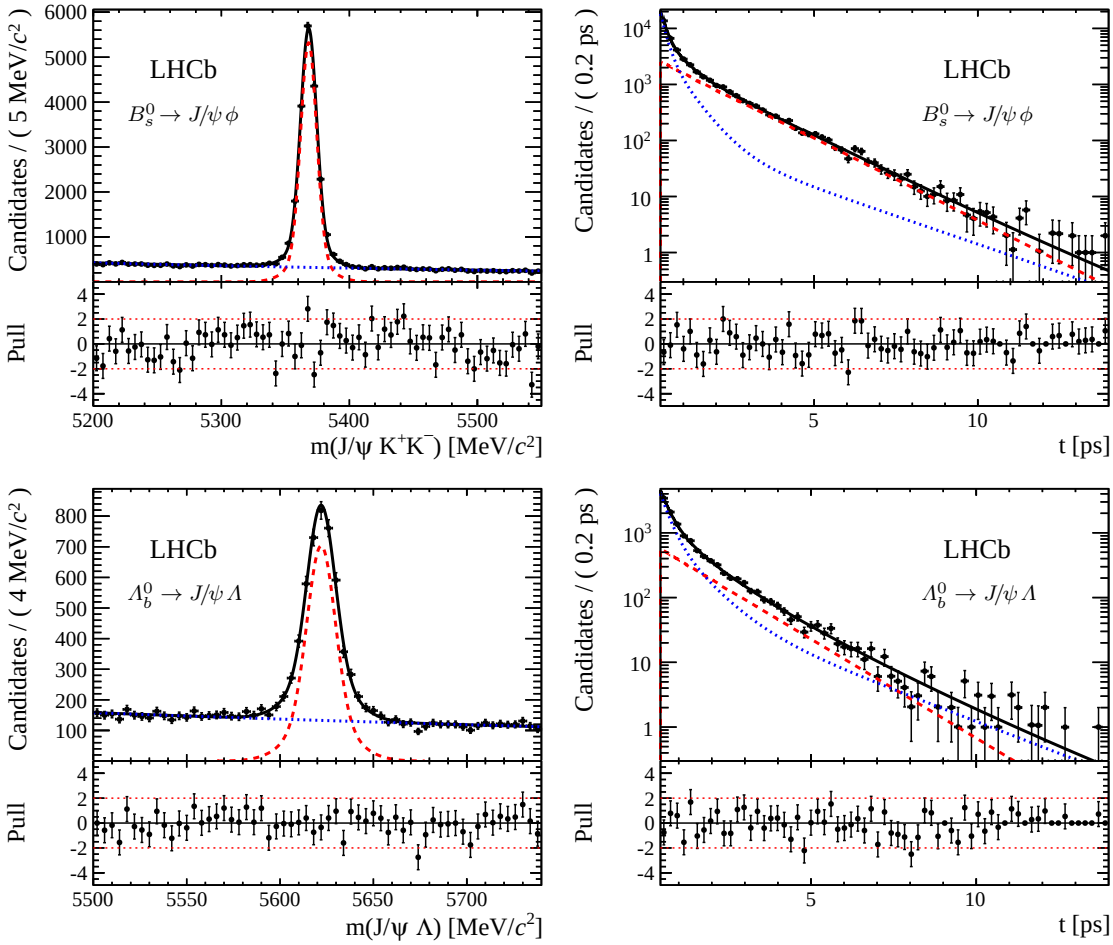

Figure 2: Distributions of the (left) mass and (right) decay time of $B_s^0 \to J/\psi\,\phi$ and $\Lambda_b^0 \to J/\psi\,\Lambda$ candidates and their associated residual uncertainties (pulls). The data are shown by the black points; the total fit function by the black solid line; the signal contribution by the red dashed line and the background contribution by the blue dotted line.

Table 2: Estimated event yields for the five $b \to J/\psi X$ channels selected using the criteria described in Sec. 3.1 to 3.5.

Channel	Yield
$B^+ \to J/\psi K^+$	$229\,434 \pm 503$
$B^0 \to J/\psi K^{*0}$	$70\,534 \pm 312$
$B^0 \to J/\psi K^0_{\rm S}$	$17\,045 \pm 175$
$B^0_s \to J/\psi \phi$	$18\,662 \pm 152$
$\Lambda^0_b \to J/\psi \Lambda$	$3\,960 \pm 89$

3.1 Selection of $B^+ \to J/\psi K^+$ decays

The B^+ candidates are reconstructed by combining the J/ψ candidates with a charged particle that is identified as a kaon with $p_{\rm T}$ larger than $1\,{\rm GeV}/c$ and p larger than $10\,{\rm GeV}/c$. The invariant mass, $m(J/\psi K^+)$, must be in the range $[5170, 5400]\,{\rm MeV}/c^2$, where the lower bound is chosen to remove feed-down from incompletely reconstructed $B^0 \to J/\psi K^{*0}$ decays. The $\chi^2_{\rm DTF}$ of the fit, which has 5 degrees of freedom, is required to be less than 25. Multiple B^+ candidates are found in less than 0.02% of selected events.

3.2 Selection of $B^0 \to J/\psi K^{*0}$ decays

The K^{*0} candidates are reconstructed by combining two oppositely charged particles that are identified as a kaon and a pion. The pion and K^{*0} must have $p_{\rm T}$ greater than $0.3\,{\rm GeV}/c$ and $1.5\,{\rm GeV}/c$, respectively. The invariant mass, $m(K^+\pi^-)$, must be in the range $[826, 966]\,{\rm MeV}/c^2$.

The B^0 candidates are reconstructed by combining the J/ψ and K^{*0} candidates. The invariant mass, $m(J/\psi K^+\pi^-)$, must be in the range $[5150, 5340]\,{\rm MeV}/c^2$, where the upper bound is chosen to remove the contribution from $B^0_s \to J/\psi \overline{K}^{*0}$ decays. The $\chi^2_{\rm DTF}$ of the fit, which has 3 degrees of freedom, is required to be less than 15. Multiple B^0 candidates are found in 2.2% of selected events.

3.3 Selection of $B^0 \to J/\psi K^0_{\rm S}$ decays

The $K^0_{\rm S}$ candidates are formed from the combination of two oppositely charged particles that are identified as pions and reconstructed as downstream tracks. This is necessary since studies of simulated signal decays demonstrate that an inefficiency depending on the b-hadron decay time is introduced by the reconstruction of the long-lived $K^0_{\rm S}$ and Λ particles using long tracks. Even so, it is found that the acceptance of the TT still depends on the origin of the tracks. This effect is removed by further tightening of the requirement on the position of the PV to $z_{\rm PV} > -50\,{\rm mm}$.

For particles produced close to the interaction region, this effect is suppressed by the requirements on the fiducial region for the PV, which is further tightened by requiring

that , to account for the additional acceptance introduced by the TT.

The downstream pions are required to have $p_{\rm T}$ greater than $0.1\,{\rm GeV}/c$ and p greater than $2\,{\rm GeV}/c$. The $K^0_{\rm S}$ candidate must have $p_{\rm T}$ greater than $1\,{\rm GeV}/c$ and be well separated from the B^0 decay vertex, to suppress potential background from $B^0 \to J/\psi\, K^{*0}$ decays where the kaon has been misidentified as a pion. The χ^2 of the $K^0_{\rm S}$ vertex fit must be less than 25 and the invariant mass of the dipion system, $m(\pi^+\pi^-)$, must be within $15\,{\rm MeV}/c^2$ of the known $K^0_{\rm S}$ mass [44]. For subsequent stages of the selection, $m(\pi^+\pi^-)$ is constrained to the known $K^0_{\rm S}$ mass.

The invariant mass, $m(J/\psi\, K^0_{\rm S})$, of the J/ψ and $K^0_{\rm S}$ candidate combination must be in the range $[5150, 5340]\,{\rm MeV}/c^2$, where the upper bound is chosen to remove the contribution from $B^0_s \to J/\psi\, K^0_{\rm S}$ decays. The $\chi^2_{\rm DTF}$ of the fit, which has 6 degrees of freedom, is required to be less than 30. Multiple B^0 candidates are found in less than 0.4% of selected events.

3.4 Selection of $B^0_s \to J/\psi\,\phi$ decays

The ϕ candidates are formed from two oppositely charged particles that have been identified as kaons and originate from a common vertex. The K^+K^- pair is required to have $p_{\rm T}$ larger than $1\,{\rm GeV}/c$. The invariant mass of the K^+K^- pair, $m(K^+K^-)$, must be in the range $[990, 1050]\,{\rm MeV}/c^2$.

The B^0_s candidates are reconstructed by combining the J/ψ candidate with the K^+K^- pair, requiring the invariant mass, $m(J/\psi\, K^+K^-)$, to be in the range $[5200, 5550]\,{\rm MeV}/c^2$. The $\chi^2_{\rm DTF}$ of the fit, which has 3 degrees of freedom, is required to be less than 15. Multiple B^0_s candidates are found in less than 2.0% of selected events.

3.5 Selection of $\Lambda^0_b \to J/\psi\,\Lambda$ decays

The selection of $\Lambda^0_b \to J/\psi\,\Lambda$ candidates follows a similar approach to that adopted for $B^0 \to J/\psi\, K^0_{\rm S}$ decays. Only downstream protons and pions are used to reconstruct the Λ candidates. The pions are required to have $p_{\rm T}$ larger than $0.1\,{\rm GeV}/c$, while pions and protons must have p larger than $2\,{\rm GeV}/c$. The Λ candidate must be well separated from the Λ^0_b decay vertex and have $p_{\rm T}$ larger than $1\,{\rm GeV}/c$. The χ^2 of the Λ vertex fit must be less than 25 and $m(p\pi^-)$ must be within $6\,{\rm MeV}/c^2$ of the known Λ mass [44]. For subsequent stages of the selection, $m(p\pi^-)$ is constrained to the known Λ mass.

The invariant mass, $m(J/\psi\,\Lambda)$, of the J/ψ and Λ candidate combination must be in the range $[5470, 5770]\,{\rm MeV}/c^2$. The $\chi^2_{\rm DTF}$ of the fit, which has 6 degrees of freedom, is required to be less than 30. Multiple Λ^0_b candidates are found in less than 0.5% of selected events.

4 Dependence of efficiencies on decay time

Section 3 described the reconstruction and selection criteria of the $H_b \to J/\psi\, X$ decays and various techniques that have been used to minimise the dependence of selection efficiencies upon the decay time. After these steps, there remain two effects that distort the b-hadron

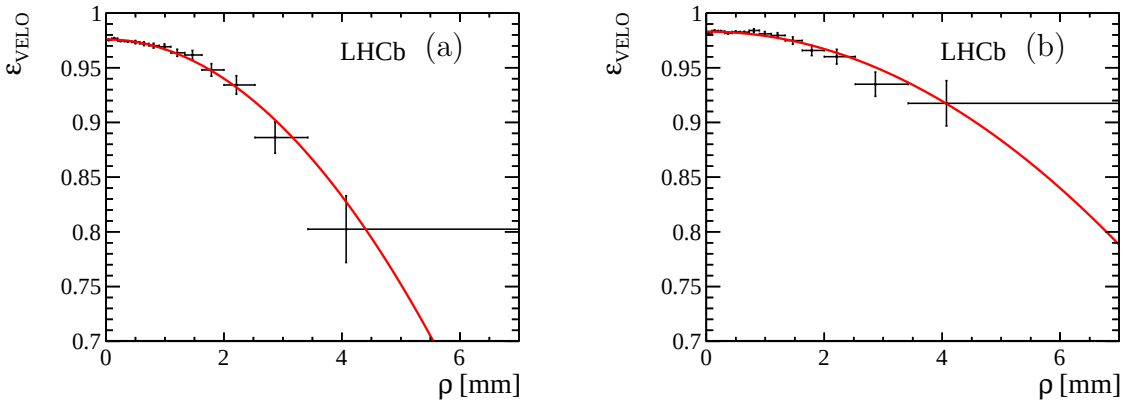

Figure 3: VELO-track reconstruction efficiency for kaon tracks reconstructed using the (a) online and (b) offline algorithms as a function of the kaon ρ, as defined in Eq. (3). The red solid lines show the result of an unbinned maximum likelihood fit using the parameterisation in Eq. (4) to the background subtracted data (black points).

decay time distribution. These are caused by the VELO-track reconstruction efficiency, $\varepsilon_{\rm VELO}$, and the combination of the trigger efficiency, $\varepsilon_{\rm trigger}$, and offline selection efficiency, $\varepsilon_{\rm selection|trigger}$. This section will describe these effects and the techniques that are used to evaluate the efficiencies from data control samples.

4.1 VELO-track reconstruction efficiency

The largest variation of the efficiency with the decay time is introduced by the track reconstruction in the VELO. The track finding procedure in the VELO assumes that tracks originate approximately from the interaction region [33, 45]. In the case of long-lived b-hadron candidates this assumption is not well justified, leading to a loss of reconstruction efficiency for charged particle tracks from the b-hadron decay.

The distance of closest approach of the track to the z-axis is defined as

$$\rho \equiv \frac{|(\boldsymbol{d}-\boldsymbol{v})\cdot(\boldsymbol{p}\times\hat{\boldsymbol{z}})|}{|\boldsymbol{p}\times\hat{\boldsymbol{z}}|}, \tag{3}$$

where $\boldsymbol{p}$ is the momentum of the final-state track from a b-hadron candidate decaying at point $\boldsymbol{d}$, $\hat{\boldsymbol{z}}$ is a unit vector along the z-axis and $\boldsymbol{v}$ is the origin of the VELO coordinate system. During data taking the position of the LHCb VELO is monitored as a function of time and is centred around the LHC beam line. Using a control sample of $B^+ \to J/\psi K^+$ candidates where the K^+ is reconstructed as a downstream track, the VELO-track reconstruction efficiency, $\varepsilon_{\rm VELO}(\rho)$, is computed as the fraction of these tracks that are also reconstructed as long tracks. From samples of simulated b-hadron decays, it is observed that $\varepsilon_{\rm VELO}(\rho)$ can be empirically parameterised by

$$\varepsilon_{\rm VELO}(\rho) = a(1+c\rho^2), \tag{4}$$

Table 3: VELO reconstruction efficiency in data for kaon tracks reconstructed with the online and offline algorithms. In both cases, the correlation coefficient between a and c is 0.2.

	a	$c\,[\mathrm{mm}^{-2}]$
Online	0.9759 ± 0.0005	-0.0093 ± 0.0007
Offline	0.9831 ± 0.0004	-0.0041 ± 0.0005

where the parameters a and c are determined from a fit to the unbinned efficiency distribution.

Figure 3 shows the VELO-track reconstruction efficiency obtained using this method and Table 3 shows the corresponding fit results. Since different configurations of the VELO reconstruction algorithms are used within the LHCb software trigger (online) and during the subsequent processing (offline), it is necessary to evaluate two different efficiencies. The stronger dependence of the online efficiency as a function of ρ is due to the additional requirements used in the first stage of the software trigger such that it satisfies the required processing time.

Applying the same technique to a simulated sample of $B^+ \to J/\psi\, K^+$ decays yields qualitatively similar behaviour for $\varepsilon_{\mathrm{VELO}}(\rho)$. Studies on simulated data show that the efficiency for kaons and pions from the decay of ϕ and K^{*0} mesons is smaller than for the kaon in $B^+ \to J/\psi\, K^+$ decays, due to the small opening between the particles in the ϕ and K^{*0} decays, as discussed in Sec. 3. In addition, there are kinematic differences between the calibration B^+ sample and the signal samples. Scaling factors on the efficiency parameters are derived from simulation to account for these effects, and have typical sizes in the range $[1.04, 1.65]$, depending on the decay mode and final-state particle being considered.

The distortion to the b-hadron candidate decay time distribution caused by the VELO-track reconstruction is corrected for by weighting each b-hadron candidate by the inverse of the product of the per-track efficiencies. The systematic effect introduced by this weighting is tested using simulated samples of each channel. The chosen efficiency depends on whether the particle is reconstructed with the online or offline variant of the algorithm. Studies on simulated data show that tracks found by the online tracking algorithm are also found by the offline tracking efficiency. For example, the efficiency weight for each $B^0 \to J/\psi\, K^{*0}$ candidate takes the form

$$w_{B^0 \to J/\psi\, K^{*0}} \;=\; 1/\left(\varepsilon^{\mu^+}_{\mathrm{VELO,online}}\; \varepsilon^{\mu^-}_{\mathrm{VELO,online}}\; \varepsilon^{K^+}_{\mathrm{VELO,offline}}\; \varepsilon^{\pi^-}_{\mathrm{VELO,offline}}\right), \tag{5}$$

since the two muons are required to be reconstructed online, while the kaons and the pions are reconstructed offline.

In the case of the $B^0 \to J/\psi\, K^0_{\mathrm{S}}$ and $\Lambda^0_b \to J/\psi\, \Lambda$ channels, since no VELO information is used when reconstructing the K^0_{S} and Λ particles, the candidate weighting functions take the form $w = 1/\left(\varepsilon^{\mu^+}_{\mathrm{VELO,online}}\; \varepsilon^{\mu^-}_{\mathrm{VELO,online}}\right)$.

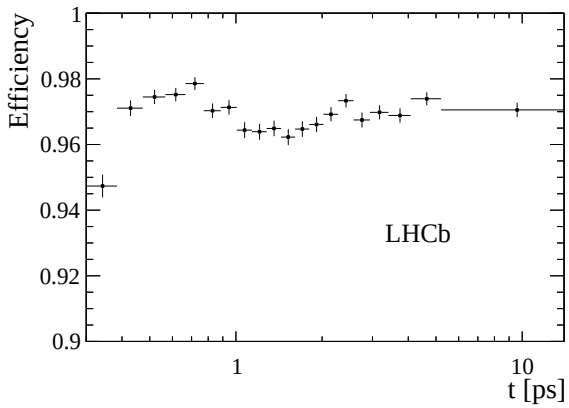

Figure 4: Combined trigger and selection efficiency, $\varepsilon_{\text{selection}}(t)$, for $B^+ \to J/\psi K^+$ candidates.

4.2 Trigger and selection efficiency

The efficiency of the second stage of the software trigger depends on the b-hadron decay time as it requires that the J/ψ meson is significantly displaced from the PV. A parameterisation of this efficiency, $\varepsilon_{\text{trigger}}(t)$, is obtained for each $b \to J/\psi X$ decay mode by exploiting a corresponding sample of $b \to J/\psi X$ candidates that are selected without any displacement requirement. For each channel, the control sample corresponds to approximately 40% of the total number of signal candidates. A maximum likelihood fit to the unbinned invariant mass distribution $m(J/\psi X)$ is performed to determine the fraction of signal decays that survive the decay-time biasing trigger requirements as a function of decay time.

The same technique is used to determine the decay time efficiency of the triggered candidates caused by the offline selection, $\varepsilon_{\text{selection|trigger}}(t)$, which is introduced by the requirement on the detachment of the J/ψ mesons in the sample used to reconstruct the b-hadron decays. The combined selection efficiency, $\varepsilon_{\text{selection}}(t)$, is given by the product of $\varepsilon_{\text{trigger}}(t)$ and $\varepsilon_{\text{selection|trigger}}(t)$.

Figure 4 shows $\varepsilon_{\text{selection}}(t)$ obtained for the $B^+ \to J/\psi K^+$ channel as a function of decay time. The efficiencies obtained for the other $H_b \to J/\psi X$ channels are qualitatively similar. Studies using simulated events show that the efficiency drop below 0.5 ps is caused by the J/ψ displacement requirement. The dip near 1.5 ps appears because the PV reconstruction in the software trigger is such that some final-state tracks of short-lived b-hadron decays may be used to reconstruct an additional fake PV close to the true b-hadron decay vertex. As a result the reconstructed J/ψ meson does not satisfy the displacement requirement, leading to a decrease in efficiency.

The efficiency parameterisation for each channel is used in the fit to measure the corresponding b-hadron lifetime. An exception is made for the $\Lambda_b^0 \to J/\psi \Lambda$ channel where, owing to its smaller event yield, $\varepsilon_{\text{selection}}(t)$ measured with $B^0 \to J/\psi K_S^0$ decays is used instead. The validity of this approach is checked using large samples of simulated events.

5 Maximum likelihood fit

For each channel, the lifetime is determined from a two-dimensional maximum likelihood fit to the unbinned $m(J/\psi X)$ and t distributions. The full probability density function (PDF) is constructed as $\mathcal{P} = f_s(\mathcal{S}_m \times \mathcal{S}_t) + (1 - f_s)(\mathcal{B}_m \times \mathcal{B}_t)$, where f_s is the signal fraction, determined in the fit, and $\mathcal{S}_m \times \mathcal{S}_t$ and $\mathcal{B}_m \times \mathcal{B}_t$ are the $(m(J/\psi X), t)$ PDFs for the signal and background components, respectively. A systematic uncertainty is assigned to the assumption that the PDFs factorise.

The signal mass PDF, $\mathcal{S}_m$, is modelled by the sum of two Gaussian functions. The free parameters in the fit are the common mean, the width of the narrower Gaussian function, the ratio of the second to the first Gaussian width and the fraction of the first Gaussian function. The background mass distribution, $\mathcal{B}_m$, is modelled by an exponential function with a single free parameter.

The signal b-hadron decay time distribution is described by an exponential function with decay constant given by the b-hadron lifetime, $\tau_{H_b \to J/\psi X}$. The signal decay time PDF, $\mathcal{S}_t$, is obtained by multiplying the exponential function by the combined t-dependent trigger and selection efficiency described in Sec. 4.2. From inspection of events in the sidebands of the b-hadron signal peak, the background decay time PDF, $\mathcal{B}_t$, is well modelled by a sum of three exponential functions with different decay constants that are free in the fit. These components originate from a combination of prompt candidates, where all tracks originate from the same PV, and long-lived candidates where tracks from the associated PV are combined with other tracks of long-lived particles. For each channel the exponential functions are convolved with a Gaussian resolution function with width σ and mean Δ, an offset of the order of a few femtoseconds that is fixed in the fit. Using a sample of prompt J/ψ background events, the decay time resolution for $H_b \to J/\psi X$ channels reconstructed using long tracks has been measured to be approximately 45 fs [46]. For $B^0 \to J/\psi K^0_S$ and $\Lambda^0_b \to J/\psi \Lambda$ decays, which use downstream tracks to reconstruct the K^0_S and Λ particles, a similar study of an event sample composed of prompt J/ψ mesons combined with two downstream tracks, reconstructed as either a K^0_S or Λ, has determined the resolution to be 65 fs. The systematic uncertainties related to the choice of resolution model are discussed in Sec. 6.

The negative log-likelihood, constructed as

$$-\ln \mathcal{L} = -\alpha \sum_{\text{events } i} w_i \ln \mathcal{P}, \tag{6}$$

is minimised in the fit, where the weights w_i correspond to the per-candidate correction for the VELO reconstruction efficiency described in Sec. 4.1. The factor $\alpha = \sum_i w_i / \sum_i w_i^2$ is used to include the effect of the weights in the determination of the uncertainties [47]. Figures 1 and 2 show the result of fitting this model to the selected candidates for each channel, projected onto the corresponding $m(J/\psi X)$ and t distributions.

As a consistency check, an alternative fit procedure is developed where each event is given a signal weight, W_i, determined using the *sPlot* [48] method with $m(J/\psi X)$ as the discriminating variable and using the mass model described above. A weighted fit to the

decay time distribution using the signal PDF is then used to measure the b-hadron lifetime. In this case, the negative log-likelihood is given by Eq. (6) where w_i is replaced with $W_i w_i$ and $\alpha = \sum_i (W_i w_i) / \sum_i (W_i w_i)^2$. The difference between the results of the two fitting procedures is used to estimate the systematic uncertainty on the background description.

6 Systematic uncertainties

The systematic effects affecting the measurements reported here are discussed in the following and summarised in Tables 4 and 5.

The systematic uncertainty related to the VELO-track reconstruction efficiency can be split into two components. The first uncertainty is due to the finite size of the $B^+ \to J/\psi K^+$ sample, reconstructed using downstream kaon tracks, which is used to determine the per-candidate efficiency weights and leads to a statistical uncertainty on the $\varepsilon_{\rm VELO}(\rho)$ parameterisation. The lifetime fits are repeated after varying the parameters by $\pm 1\sigma$ and the largest difference between the lifetimes is assigned as the uncertainty. The second uncertainty is due to the scaling factors, which are used to correct the efficiency for phase-space effects, obtained from simulated events. The fit is repeated using the unscaled efficiency and half of the variation in fit results is assigned as a systematic uncertainty. These contributions, of roughly the same size, are added in quadrature in Table 4.

A number of additional consistency checks are performed to investigate possible mismodelling of the VELO-track reconstruction efficiency. First, $\varepsilon_{\rm VELO}(\rho)$ is evaluated in two track momentum and two track multiplicity bins and the event weights recalculated. Using both data and simulated events, no significant change in the lifetimes is observed after repeating the fit with the updated weights and, therefore, no systematic uncertainty is assigned. Secondly, to assess the sensitivity to the choice of parameterisation for $\varepsilon_{\rm VELO}(\rho)$ (Eq. 4), the results are compared to those with linear model for the efficiency. The effect is found to be negligible and no systematic uncertainty is applied. Thirdly, the dependence of the VELO-track reconstruction efficiency on the azimuthal angle, ϕ, of each track is studied by independently evaluating the efficiency in four ϕ quadrants for both data and simulation. No dependence is observed. Finally, the efficiency is determined separately for both positive and negative kaons and found to be compatible.

The techniques described in Sec. 4 to correct the efficiency as a function of the decay time are validated on simulated data. The lifetime is fit in each simulated signal mode and the departure from the generated lifetime, $\Delta\tau$, is found to be compatible with zero within the statistical precision of each simulated sample. The measured lifetimes in the data sample are corrected by each $\Delta\tau$ and a corresponding systematic uncertainty is assigned, given by the size of the statistical uncertainty on the fitted lifetime for each simulated signal mode.

The assumption that $m(J/\psi X)$ is independent of the decay time is central to the validity of the likelihood fits used in this study. It is tested by re-evaluating the signal weights of the alternative fit in bins of decay time and then refitting the entire sample using the modified weights. The systematic uncertainty for each decay mode is evaluated

as the sum in quadrature of the lifetime variations, each weighted by the fraction of signal events in the corresponding bin.

For each signal decay mode, the effect of the limited size of the control sample used to estimate the combined trigger and selection efficiency is evaluated by repeating the fits with $\varepsilon_{\text{selection}}(t)$ randomly fluctuated within its statistical uncertainty. The standard deviation of the distribution of lifetimes obtained is assigned as the systematic uncertainty.

The alternative likelihood fit does not assume any model for the decay time distribution associated with the combinatorial background. Therefore, the systematic uncertainty associated to the modelling of this background is evaluated by taking the difference in lifetimes measured by the nominal and alternative fit methods.

The fit uses a double Gaussian function to describe the $m(J/\psi X)$ distribution of signal candidates. This assumption is tested by repeating the fit using a double-sided Apollonios function [49] where the mean and width parameters are varied in the fit and the remaining parameters are fixed to those from simulation. The differences in lifetime with respect to the default results are taken as systematic uncertainties.

As described in Sec. 5 the dominant background in each channel is combinatorial in nature. It is also possible for backgrounds to arise due to misreconstruction of b-hadron decays where the particle identification has failed. The presence of such backgrounds is checked by inspecting events in the sidebands of the signal and re-assigning the mass hypotheses of at least one of the final-state hadrons. The only contributions that have an impact are $\Lambda_b^0 \to J/\psi p K^-$ decays in the $B_s^0 \to J/\psi\,\phi$ channel where a proton is misidentified as a kaon and the cross-feed component between $B^0 \to J/\psi\, K^0_{\rm S}$ and $\Lambda_b^0 \to J/\psi\,\Lambda$ decays where pion and protons are misidentified. In the case of $B_s^0 \to J/\psi\,\phi$ decays, the fit is repeated including a contribution of $\Lambda_b^0 \to J/\psi p K^-$ decays. The two-dimensional PDF is determined from simulation, while the yield is found to be 6% from the sidebands of the B_s^0 sample. This leads to the effective lifetime changing by 0.4 fs, which is assigned as a systematic uncertainty. A similar procedure is used to determine the invariant mass shape of the cross-feed background between $B^0 \to J/\psi\, K^0_{\rm S}$ and $\Lambda_b^0 \to J/\psi\,\Lambda$ decays, while the decay time is modelled with the exponential distribution of the corresponding signal mode. A simultaneous fit to both data samples is performed in order to constrain the yield of the cross-feed and the resulting change in lifetime of -0.3 fs and $+1.1$ fs for B^0 and Λ_b^0, respectively, is assigned as a systematic uncertainty.

Another potential source of background is the incorrect association of signal b hadrons to their PV, which results in an erroneous reconstruction of the decay time. Since the fitting procedure ignores this contribution, a systematic uncertainty is evaluated by repeating the fit after including in the background model a component describing the incorrectly associated candidates. The background distribution is determined by calculating the decay time for each $B^+ \to J/\psi\, K^+$ decay with respect to a randomly chosen PV from the previous selected event. In studies of simulated events the fraction of this background is less than 0.1%. Repeating the fit with a 1% contribution results in the lifetime changing by 0.1 fs and, therefore, no systematic uncertainty is assigned.

The measurement of the effective lifetime in the $B_s^0 \to J/\psi\,\phi$ channel is integrated over the angular distributions of the final-state particles and is, in the case of uniform angular

efficiency, insensitive to the different polarisations of the final state [46]. To check if the angular acceptance introduced by the detector geometry and event selection can affect the measured lifetime, the events are weighted by the inverse of the angular efficiency determined in Ref. [46]. Repeating the fit with the weighted dataset leads to a shift of the lifetime of $-1.0\,\text{fs}$, the same as is observed in simulation. The final result is corrected by this shift, which is also assigned as a systematic uncertainty. The B_s^0 effective lifetime could also be biased due to a small CP-odd S-wave component from $B_s^0 \to J/\psi\, K^+K^-$ decays that is ignored in the fit. For the $m(K^+K^-)$ mass range used here (Sec. 3), Ref. [50] indicates that the S-wave contribution is 1.1%. The effect of ignoring such a component is evaluated by repeating the fit on simulated experiments with an additional 1% CP-odd component. A change in the lifetime of $-1.2\,\text{fs}$ is observed, which is used to correct the final lifetime and is also taken as a systematic uncertainty. Finally, as described in Sec. 3, only events with a decay time larger than 0.3 ps are considered in the nominal fit. This offset leads to a different relative contribution of the heavy and light mass eigenstates such that the lifetime extracted from the exponential fit does not correspond to the effective lifetime defined in Eq. (2). A correction of $-0.3\,\text{fs}$ is applied to account for this effect.

The presence of a production asymmetry between B^0 and $\overline{B}^0$ mesons could bias the measured $B^0 \to J/\psi\, K^0_S$ effective lifetime, and therefore $\Delta\Gamma_d/\Gamma_d$, by adding additional terms in Eq. (2). The production asymmetry is measured to be $A_P(B^0) = (0.6 \pm 0.9)\%$ [51], the uncertainty of which is used to estimate a corresponding systematic uncertainty on the $B^0 \to J/\psi\, K^0_S$ lifetime of 1.1 fs. No uncertainty is assigned to the $B^0 \to J/\psi\, K^{*0}$ lifetime since this decay mode is flavour-specific[2] and the production asymmetry cancels in the untagged decay rate. For the B_s^0 system, the rapid oscillations, due to the large value of $\Delta m_s = 17.768 \pm 0.024\,\text{ps}^{-1}$ [52], reduce the effect of a production asymmetry, reported as $A_P(B_s^0) = (7 \pm 5)\%$ in Ref. [51], to a negligible level. Hence, no corresponding systematic uncertainty is assigned.

There is a 0.02% relative uncertainty on the lifetime measurements due to the uncertainty on the length scale of LHCb [52], which is mainly determined by the VELO modules z positions. These are evaluated by a survey, having an accuracy of 0.1 mm over the full length of the VELO (1000 mm), and refined through a track-based alignment. The alignment procedure is more precise for the first track hits, that are less affected by multiple scattering and whose distribution of z positions have an RMS of 100 mm. In this region, the differences between the module positions obtained from the survey and track-based alignment are within 0.02 mm, which is taken as systematic uncertainty. The systematic uncertainty related to the momentum scale calibration affects both the b hadron candidate mass and momentum and, therefore, cancels when computing the decay time.

The systematic uncertainty related to the choice of 45 fs for the width of the decay-time resolution function (65 fs in the case of $B^0 \to J/\psi\, K^0_S$ and $\Lambda_b^0 \to J/\psi\, \Lambda$) is evaluated by changing the width by $\pm 15\,\text{fs}$ and repeating the fit. This change in width is larger than the estimated uncertainty on the resolution and leads to a negligible change in the fit

[2]Flavour-specific means that the final state is only accessible via the decay of a $B^0_{(s)}$ meson and accessible by a meson originally produced as a $\overline{B}^0_{(s)}$ only via oscillation.

Table 4: Statistical and systematic uncertainties (in femtoseconds) for the values of the b-hadron lifetimes. The total systematic uncertainty is obtained by combining the individual contributions in quadrature.

Source	$\tau_{B^+\to J/\psi K^+}$	$\tau_{B^0\to J/\psi K^{*0}}$	$\tau_{B^0\to J/\psi K^0_S}$	$\tau_{\Lambda^0_b\to J/\psi \Lambda}$	$\tau_{B^0_s\to J/\psi \phi}$
Statistical uncertainty	3.5	6.1	12.8	26.5	11.4
VELO reconstruction	2.0	2.3	0.9	0.5	2.3
Simulation sample size	1.7	2.3	2.9	3.7	2.4
Mass-time correlation	1.4	1.8	2.1	3.0	0.7
Trigger and selection eff.	1.1	1.2	2.0	2.0	2.5
Background modelling	0.1	0.2	2.2	2.1	0.4
Mass modelling	0.1	0.2	0.4	0.2	0.5
Peaking background	–	–	0.3	1.1	0.4
Effective lifetime bias	–	–	–	–	1.6
B^0 production asym.	–	–	1.1	–	–
LHCb length scale	0.4	0.3	0.3	0.3	0.3
Total systematic	3.2	3.9	4.9	5.7	4.6

results. Consequently, no systematic uncertainty is assigned. Furthermore, to test the sensitivity of the lifetimes to potential mismodelling of the long tails in the resolution, the resolution model is changed from a single Gaussian function to a sum of two or three Gaussian functions with parameters fixed from simulation. Repeating the fit with the new resolution model causes no significant change to the lifetimes and no systematic uncertainty is assigned. The lifetimes are insensitive to the offset, Δ, in the resolution model.

Several consistency checks are performed to study the stability of the lifetimes, by comparing the results obtained using different subsets of the data in terms of magnet polarity, data taking period, b-hadron and track kinematic variables, number of PVs in the event and track multiplicity. In all cases, no trend is observed and all lifetimes are compatible with the nominal results.

The majority of the systematic uncertainties described above can be propagated to the lifetime ratio measurements in Table 7. However, some of the uncertainties are correlated between the individual lifetimes and cancel in the ratio. For the first set of ratios and for $\Delta\Gamma_d/\Gamma_d$, the systematic uncertainty from the VELO-reconstruction efficiency weights and the LHCb length scale are considered as fully correlated. For the second set of ratios, other systematic uncertainties, as indicated in Table 5, cancel, since the ratio is formed from lifetimes measured using the same decay mode. In contrast to the situation for the measurement of the B^0 lifetime in the $B^0\to J/\psi K^{*0}$ mode, the B^0 production asymmetry does lead to a systematic uncertainty on the measurement of $\tau_{B^0\to J/\psi K^{*0}}/\tau_{\overline{B}^0\to J/\psi \overline{K}^{*0}}$ since terms like $A_{\rm P}\cos(\Delta m_d t)$ do not cancel in the decay rates describing the decays of B^0 and $\overline{B}^0$ mesons to $J/\psi K^{*0}$ and $J/\psi \overline{K}^{*0}$ final states. The effect of candidates where the flavour, via the particle identification of the decay products, has not been correctly assigned is investigated and found to be negligible.

Table 5: Statistical and systematic uncertainties (in units of 10^{-3}) for the lifetime ratios and $\Delta\Gamma_d/\Gamma_d$. For brevity, τ_{B^0} ($\tau_{\overline{B}^0}$) corresponds to the measurement of $\tau_{B^0\to J/\psi K^{*0}}$ ($\tau_{\overline{B}^0\to J/\psi \overline{K}^{*0}}$). The total systematic uncertainty is obtained by combining the individual contributions in quadrature.

Source	τ_{B^+}/τ_{B^0}	$\tau_{B_s^0}/\tau_{B^0}$	$\tau_{\Lambda_b^0}/\tau_{B^0}$	τ_{B^+}/τ_{B^-}	$\tau_{\Lambda_b^0}/\tau_{\overline{\Lambda}_b^0}$	$\tau_{B^0}/\tau_{\overline{B}^0}$	$\Delta\Gamma_d/\Gamma_d$
Statistical uncertainty	5.0	8.5	18.0	4.0	35.0	8.0	25.0
VELO reconstruction	1.6	1.7	1.1	–	–	–	4.1
Simulation sample size	2.0	2.2	2.8	2.1	5.3	3.0	6.3
Mass-time correlation	1.6	1.2	2.3	–	–	–	4.7
Trigger and selection eff.	1.1	1.8	1.5	–	–	–	4.0
Background modelling	0.3	0.1	1.5	0.2	3.0	1.4	3.8
Mass modelling	0.2	0.4	0.2	0.1	0.2	0.2	0.8
Peaking background	–	0.3	0.7	–	–	–	0.5
Effective lifetime bias	–	1.0	–	–	–	–	–
B^0 production asym.	–	–	–	–	–	8.5	1.9
Total systematic	3.2	3.7	4.4	2.1	6.1	9.1	10.7

Table 6: Fit results for the B^+, B^0, B_s^0 mesons and Λ_b^0 baryon lifetimes. The first uncertainty is statistical and the second is systematic.

Lifetime	Value [ps]
$\tau_{B^+\to J/\psi K^+}$	$1.637 \pm 0.004 \pm 0.003$
$\tau_{B^0\to J/\psi K^{*0}}$	$1.524 \pm 0.006 \pm 0.004$
$\tau_{B^0\to J/\psi K^0_S}$	$1.499 \pm 0.013 \pm 0.005$
$\tau_{\Lambda_b^0\to J/\psi \Lambda}$	$1.415 \pm 0.027 \pm 0.006$
$\tau_{B_s^0\to J/\psi \phi}$	$1.480 \pm 0.011 \pm 0.005$

7 Results and conclusions

The measured b-hadron lifetimes are reported in Table 6. All results are compatible with existing world averages [13]. The reported $\tau_{\Lambda_b^0\to J/\psi\Lambda}$ is smaller by approximately 2σ than a previous measurements from LHCb [8]. With the exception of the $\Lambda_b^0\to J/\psi\Lambda$ channel, these are the single most precise measurements of the b-hadron lifetimes. The B_s^0 meson effective lifetime is measured using the same data set as used in Ref. [46] for the measurement of the B_s^0 meson mixing parameters and polarisation amplitudes in $B_s^0\to J/\psi\phi$ decays. The B_s^0 meson effective lifetime computed from these quantities is compatible with the lifetime reported in this paper and a combination of the two results is, therefore, inappropriate.

Table 7 reports the ratios of the B^+, B_s^0 and Λ_b^0 lifetimes to the B^0 lifetime measured in the flavour-specific $B^0\to J/\psi K^{*0}$ channel. This decay mode provides a better normalisation than the $B^0\to J/\psi K^0_S$ channel due to the lower statistical uncertainty on the B^0 meson lifetime and due to the fact that the $B^0\to J/\psi K^{*0}$ lifetime only depends quadratically on $\Delta\Gamma_d/\Gamma_d$, as shown in Eq. (7). The statistical and systematic uncertainties from

Table 7: Lifetime ratios for the B^+, B^0, B_s^0 mesons and Λ_b^0 baryon. The first uncertainty is statistical and the second is systematic.

Ratio	Value
$\tau_{B^+}/\tau_{B^0\to J/\psi K^{*0}}$	$1.074 \pm 0.005 \pm 0.003$
$\tau_{B_s^0}/\tau_{B^0\to J/\psi K^{*0}}$	$0.971 \pm 0.009 \pm 0.004$
$\tau_{\Lambda_b^0}/\tau_{B^0\to J/\psi K^{*0}}$	$0.929 \pm 0.018 \pm 0.004$
τ_{B^+}/τ_{B^-}	$1.002 \pm 0.004 \pm 0.002$
$\tau_{\Lambda_b^0}/\tau_{\overline{\Lambda}_b^0}$	$0.940 \pm 0.035 \pm 0.006$
$\tau_{B^0\to J/\psi K^{*0}}/\tau_{\overline{B}^0\to J/\psi \overline{K}^{*0}}$	$1.000 \pm 0.008 \pm 0.009$

the absolute lifetime measurements are propagated to the ratios, taking into account the correlations between the systematic uncertainties. All ratios are consistent with SM predictions [15,22–25,30–32] and with previous measurements [13]. Furthermore, the ratios τ_{B^+}/τ_{B^-}, $\tau_{\Lambda_b^0}/\tau_{\overline{\Lambda}_b^0}$ and $\tau_{B^0\to J/\psi K^{*0}}/\tau_{\overline{B}^0\to J/\psi \overline{K}^{*0}}$ are reported. Measuring any of these different from unity would indicate a violation of *CPT* invariance or, for $B^0 \to J/\psi K^{*0}$ decays, could also indicate that $\Delta\Gamma_d$ is non-zero and $B^0 \to J/\psi K^{*0}$ is not 100% flavour-specific. No deviation from unity of these ratios is observed.

The effective lifetimes of $B^0 \to J/\psi K^{*0}$ and $B^0 \to J/\psi K_S^0$ decays are used to measure $\Delta\Gamma_d/\Gamma_d$. Flavour-specific final states such as $B^0 \to J/\psi K^{*0}$ have $\mathcal{A}_{\Delta\Gamma_d}^{B^0\to J/\psi K^{*0}} = 0$, while $\mathcal{A}_{\Delta\Gamma_d}^{B^0\to J/\psi K_S^0} = \cos(2\beta)$ to a good approximation in the SM, where $\beta \equiv \arg\left[-(V_{cd}V_{cb}^*)/(V_{td}V_{tb}^*)\right]$ is one of the CKM unitarity triangle angles. Hence, the two effective lifetimes can be expressed as

$$\tau_{B^0\to J/\psi K^{*0}} = \frac{1}{\Gamma_d}\frac{1}{1-y_d^2}\left(1+y_d^2\right), \tag{7}$$

$$\tau_{B^0\to J/\psi K_S^0} = \frac{1}{\Gamma_d}\frac{1}{1-y_d^2}\left(\frac{1+2\cos(2\beta)y_d+y_d^2}{1+\cos(2\beta)y_d}\right). \tag{8}$$

Using the effective lifetimes reported in Table 6 and $\beta = (21.5^{+0.8}_{-0.7})^\circ$ [13], a fit of $\Delta\Gamma_d$ and Γ_d to the expressions in Eq. (7) and Eq. (8) leads to

$$\Gamma_d = \quad 0.656 \pm 0.003 \pm 0.002\,\text{ps}^{-1}, \tag{9}$$

$$\Delta\Gamma_d = -0.029 \pm 0.016 \pm 0.007\,\text{ps}^{-1}, \tag{10}$$

where the first uncertainty is statistical and the second is systematic. The correlation coefficient between $\Delta\Gamma_d$ and Γ_d is 0.43 when including statistical and systematic uncertainties. The combination gives

$$\frac{\Delta\Gamma_d}{\Gamma_d} = -0.044 \pm 0.025 \pm 0.011, \tag{11}$$

consistent with the SM expectation [14, 15] and the current world-average value [13].

Acknowledgements

We express our gratitude to our colleagues in the CERN accelerator departments for the excellent performance of the LHC. We thank the technical and administrative staff at the LHCb institutes. We acknowledge support from CERN and from the national agencies: CAPES, CNPq, FAPERJ and FINEP (Brazil); NSFC (China); CNRS/IN2P3 and Region Auvergne (France); BMBF, DFG, HGF and MPG (Germany); SFI (Ireland); INFN (Italy); FOM and NWO (The Netherlands); SCSR (Poland); MEN/IFA (Romania); MinES, Rosatom, RFBR and NRC "Kurchatov Institute" (Russia); MinECo, XuntaGal and GENCAT (Spain); SNSF and SER (Switzerland); NAS Ukraine (Ukraine); STFC (United Kingdom); NSF (USA). We also acknowledge the support received from the ERC under FP7. The Tier1 computing centres are supported by IN2P3 (France), KIT and BMBF (Germany), INFN (Italy), NWO and SURF (The Netherlands), PIC (Spain), GridPP (United Kingdom). We are indebted to the communities behind the multiple open source software packages we depend on. We are also thankful for the computing resources and the access to software R&D tools provided by Yandex LLC (Russia).

References

[1] V. A. Khoze and M. A. Shifman, *Heavy quarks*, Sov. Phys. Usp. **26** (1983) 387.

[2] M. A. Shifman and M. Voloshin, *Preasymptotic effects in inclusive weak decays of charmed particles*, Sov. J. Nucl. Phys. **41** (1985) 120.

[3] M. A. Shifman and M. Voloshin, *Hierarchy of lifetimes of charmed and beautiful hadrons*, Sov. Phys. JETP **64** (1986) 698.

[4] I. I. Bigi, N. Uraltsev, and A. Vainshtein, *Nonperturbative corrections to inclusive beauty and charm decays: QCD versus phenomenological models*, Phys. Lett. **B293** (1992) 430, `arXiv:hep-ph/9207214`.

[5] I. I. Bigi, *The QCD perspective on lifetimes of heavy-flavor hadrons*, `arXiv:hep-ph/9508408`.

[6] N. Uraltsev, *Heavy quark expansion in beauty and its decays*, `arXiv:hep-ph/9804275`.

[7] M. Neubert, *B decays and the heavy-quark expansion*, Adv. Ser. Direct. High Energy Phys. **15** (1998) 239, `arXiv:hep-ph/9702375`.

[8] LHCb collaboration, R. Aaij *et al.*, *Precision measurement of the Λ_b^0 baryon lifetime*, Phys. Rev. Lett. **111** (2013) 102003, `arXiv:1307.2476`.

[9] K. Hartkorn and H. Moser, *A new method of measuring $\Delta\Gamma/\Gamma$ in the B_s^0 anti-B_s^0 system*, Eur. Phys. J. **C8** (1999) 381.

[10] I. Dunietz, R. Fleischer, and U. Nierste, *In pursuit of new physics with B_s decays*, Phys. Rev. **D63** (2001) 114015, arXiv:hep-ph/0012219.

[11] R. Fleischer and R. Knegjens, *Effective lifetimes of B_s decays and their constraints on the B_s^0-$\bar{B}_s^0$ mixing parameters*, Eur. Phys. J. **C71** (2011) 1789, arXiv:1109.5115.

[12] U. Nierste, *CP asymmetry in flavor-specific B decays*, arXiv:hep-ph/0406300.

[13] Heavy Flavor Averaging Group, Y. Amhis *et al.*, *Averages of b-hadron, c-hadron, and τ-lepton properties as of early 2012*, arXiv:1207.1158, updated results and plots available at: http://www.slac.stanford.edu/xorg/hfag/.

[14] A. Lenz and U. Nierste, *Theoretical update of $B_s - \bar{B}_s$ mixing*, JHEP **06** (2007) 072, arXiv:hep-ph/0612167.

[15] A. Lenz and U. Nierste, *Numerical updates of lifetimes and mixing parameters of B mesons*, arXiv:1102.4274.

[16] BaBar collaboration, B. Aubert *et al.*, *Limits on the decay-rate difference of neutral B mesons and on CP, T, and CPT violation in $B^0\overline{B}^0$ oscillations*, Phys. Rev. Lett. **92** (2004) 181801, arXiv:hep-ex/0311037.

[17] BaBar collaboration, B. Aubert *et al.*, *Limits on the decay-rate difference of neutral B mesons and on CP, T, and CPT violation in $B^0\overline{B}^0$ oscillations*, Phys. Rev. **D70** (2004) 012007, arXiv:hep-ex/0403002.

[18] Belle collaboration, T. Higuchi *et al.*, *Search for time-dependent CPT violation in hadronic and semileptonic B decays*, Phys. Rev. **D85** (2012) 071105, arXiv:1203.0930.

[19] G. Borissov and B. Hoeneisen, *Understanding the like-sign dimuon charge asymmetry in $p\bar{p}$ collisions*, Phys. Rev. **D87** (2013) 074020, arXiv:1303.0175.

[20] D0 collaboration, V. M. Abazov *et al.*, *Study of CP-violating charge asymmetries of single muons and like-sign dimuons in $p\bar{p}$ collisions*, Phys. Rev. **D89** (2014) 012002, arXiv:1310.0447.

[21] T. Gershon, *$\Delta\Gamma_d$: a forgotten null test of the standard model*, J. Phys. **G38** (2011) 015007, arXiv:1007.5135.

[22] M. Beneke *et al.*, *The $B^+ - B_d^0$ lifetime difference beyond leading logarithms*, Nucl. Phys. **B639** (2002) 389, arXiv:hep-ph/0202106.

[23] E. Franco, V. Lubicz, F. Mescia, and C. Tarantino, *Lifetime ratios of beauty hadrons at the next-to-leading order in QCD*, Nucl. Phys. **B633** (2002) 212, arXiv:hep-ph/0203089.

[24] M. Beneke, G. Buchalla, and I. Dunietz, *Width Difference in the $B_s - \bar{B}_s$ System*, Phys. Rev. **D54** (1996) 4419, arXiv:hep-ph/9605259.

[25] Y.-Y. Keum and U. Nierste, *Probing penguin coefficients with the lifetime ratio $\tau(B_s)/\tau(B_d)$*, Phys. Rev. **D57** (1998) 4282, arXiv:hep-ph/9710512.

[26] N. Uraltsev, *On the problem of boosting nonleptonic b baryon decays*, Phys. Lett. **B376** (1996) 303, arXiv:hep-ph/9602324.

[27] I. I. Bigi, M. A. Shifman, and N. Uraltsev, *Aspects of heavy quark theory*, Ann. Rev. Nucl. Part. Sci. **47** (1997) 591, arXiv:hep-ph/9703290.

[28] D. Pirjol and N. Uraltsev, *Four fermion heavy quark operators and light current amplitudes in heavy flavor hadrons*, Phys. Rev. **D59** (1999) 034012, arXiv:hep-ph/9805488.

[29] M. Voloshin, *Reducing model dependence of spectator effects in inclusive decays of heavy baryons*, Phys. Rev. **D61** (2000) 074026, arXiv:hep-ph/9908455.

[30] C. Tarantino, *Beauty hadron lifetimes and B meson CP violation parameters from lattice QCD*, Eur. Phys. J. **C33** (2004) S895, arXiv:hep-ph/0310241.

[31] F. Gabbiani, A. I. Onishchenko, and A. A. Petrov, *Λ_b^0 lifetime puzzle in heavy quark expansion*, Phys. Rev. **D68** (2003) 114006, arXiv:hep-ph/0303235.

[32] F. Gabbiani, A. I. Onishchenko, and A. A. Petrov, *Spectator effects and lifetimes of heavy hadrons*, Phys. Rev. **D70** (2004) 094031, arXiv:hep-ph/0407004.

[33] LHCb collaboration, A. A. Alves Jr. *et al.*, *The LHCb detector at the LHC*, JINST **3** (2008) S08005.

[34] M. Adinolfi *et al.*, *Performance of the LHCb RICH detector at the LHC*, Eur. Phys. J. **C73** (2013) 2431, arXiv:1211.6759.

[35] A. A. Alves Jr *et al.*, *Performance of the LHCb muon system*, JINST **8** (2013) P02022, arXiv:1211.1346.

[36] R. Aaij *et al.*, *The LHCb trigger and its performance in 2011*, JINST **8** (2013) P04022, arXiv:1211.3055.

[37] T. Sjöstrand, S. Mrenna, and P. Skands, PYTHIA *6.4 physics and manual*, JHEP **05** (2006) 026, arXiv:hep-ph/0603175.

[38] I. Belyaev *et al.*, *Handling of the generation of primary events in* GAUSS*, the LHCb simulation framework*, Nuclear Science Symposium Conference Record (NSS/MIC) **IEEE** (2010) 1155.

[39] D. J. Lange, *The* EvtGen *particle decay simulation package*, Nucl. Instrum. Meth. **A462** (2001) 152.

[40] P. Golonka and Z. Was, Photos *Monte Carlo: a precision tool for QED corrections in Z and W decays*, Eur. Phys. J. **C45** (2006) 97, arXiv:hep-ph/0506026.

[41] Geant4 collaboration, J. Allison *et al.*, Geant4 *developments and applications*, IEEE Trans. Nucl. Sci. **53** (2006) 270; Geant4 collaboration, S. Agostinelli *et al.*, Geant4*: a simulation toolkit*, Nucl. Instrum. Meth. **A506** (2003) 250.

[42] M. Clemencic *et al.*, *The LHCb simulation application,* Gauss*: design, evolution and experience*, J. Phys.: Conf. Ser. **331** (2011) 032023.

[43] W. D. Hulsbergen, *Decay chain fitting with a Kalman filter*, Nucl. Instrum. Meth. **A552** (2005) 566, arXiv:physics/0503191.

[44] Particle Data Group, J. Beringer *et al.*, *Review of particle physics*, Phys. Rev. **D86** (2012) 010001, and 2013 partial update for the 2014 edition.

[45] O. Callot, *FastVelo, a fast and efficient pattern recognition package for the Velo*, LHCb-PUB-2011-001.

[46] LHCb collaboration, R. Aaij *et al.*, *Measurement of CP-violation and the B_s^0-meson decay width difference with $B_s^0 \to J/\psi K^+K^-$ and $B_s^0 \to J/\psi\pi^+\pi^-$ decays*, Phys. Rev. **D87** (2013) 112010, arXiv:1304.2600.

[47] Y. Xie, *sFit: a method for background subtraction in maximum likelihood fit*, arXiv:0905.0724.

[48] M. Pivk and F. R. Le Diberder, *sPlot: a statistical tool to unfold data distributions*, Nucl. Instrum. Meth. **A555** (2005) 356, arXiv:physics/0402083.

[49] D. M. Santos and F. Dupertuis, *Mass distributions marginalized over per-event errors*, submitted to Nucl. Instrum. Meth. A (2013) arXiv:1312.5000.

[50] LHCb collaboration, R. Aaij *et al.*, *Amplitude analysis and branching fraction measurement of $\overline{B}{}_s^0 \to J/\psi K^+K^-$*, Phys. Rev. **D87** (2013) 072004, arXiv:1302.1213.

[51] LHCb collaboration, R. Aaij *et al.*, *First measurement of time-dependent CP violation in $B_s^0 \to K^+K^-$ decays*, JHEP **10** (2013) 183, arXiv:1308.1428.

[52] LHCb collaboration, R. Aaij *et al.*, *Precision measurement of the $B_s^0 - \overline{B}{}_s^0$ oscillation frequency Δm_s in the decay $B_s^0 \to D_s^+\pi^-$*, New J. Phys. **15** (2013) 053021, arXiv:1304.4741.